

MRI/PET nonrigid breast-image registration using skin fiducial markers

Andrzej Krol,^{1,2,3} Mehmet Z. Unlu,² Karl G. Baum,² James A. Mandel,⁴ Wei Lee,¹
Ioana L. Coman,^{5,1,2} Edward D. Lipson,^{3,1,2} David H. Feiglin¹

1. Department of Radiology, SUNY Upstate Medical University
2. Department of Electrical Engineering and Computer Science, Syracuse University
3. Department of Physics, Syracuse University
4. Department of Civil and Environmental Engineering, Syracuse University
5. Department of Mathematics and Computer Science, Ithaca College

Abstract

We propose a finite-element method (FEM) deformable breast model that does not require elastic breast data for nonrigid PET/MRI breast image registration. The model is applicable only if the stress conditions in the imaged breast are virtually the same in PET and MRI. Under these conditions, the observed intermodality displacements are solely due the imaging/reconstruction process. Similar stress conditions are assured by use of an MRI breast-antenna replica for breast support during PET, and use of the same positioning. The tetrahedral volume and triangular surface elements are used to construct the FEM mesh from the MRI image. Our model requires a number of fiducial skin markers (FSM) visible in PET and MRI. The displacement vectors of FSMs are measured followed by the dense displacement field estimation by first distributing the displacement vectors linearly over the breast surface and then distributing them throughout the volume. Finally, the floating MRI image is warped to a fixed PET image, by using an appropriate shape function in the interpolation from mesh nodes to voxels. We tested our model on an elastic breast phantom with simulated internal lesions and on a small number of patients imaged with FSM using PET and MRI. Using simulated lesions (in phantom) and real lesions (in patients) visible in both PET and MRI, we established that the target registration error (TRE) is below two pet voxels.

KEYWORDS: Nonrigid breast image registration, Deformable FEM breast model.

1. INTRODUCTION

Breast cancer is the most common cancer among women and the second leading cause of cancer death among American women today [1]. The preferred method of breast cancer diagnosis is breast biopsy. It is performed for over 600,000 women annually [2]. It is a relatively expensive (average billed charges in USA are \$3,400 [2-3]), highly invasive, and sometimes painful procedure that can result in complications such as hematomas (7%), infection, ecchymosis, and pain (in 33-69% of patients [4]). In addition, it produces scar tissue that can complicate future mammographic examinations. Approximately 50% of breast biopsies are negative [5].

The purpose of our research is to investigate whether combined PET and MRI breast images could become a noninvasive alternative to breast biopsy, and could thereby reduce the number of retrospectively unnecessary biopsies.

Application of a multimodality approach is advantageous for detection, diagnosis and management of breast cancer. In this context, F-18-FDG positron emission tomography (PET) [6-9], and high-resolution and dynamic contrast-enhanced magnetic resonance imaging (MRI) [10-11] have steadily gained acceptance in addition to X-ray mammography and ultrasonography. Initial experiences with combined PET (physiological imaging) and CT (anatomical lo-

calization) have demonstrated sizable improvements in diagnostic accuracy, allowing better differentiation between normal (e.g. bowel) and pathological uptake and by providing positive finding in CT images for lesions with low metabolic activity [9].

The next logical step is coregistration and fusion of PET (sensitivity 68-94%, specificity 73-100%) and MRI 3-D images (sensitivity 81-96%, specificity 67-96%), to provide additional information on morphology (including borders, edema, and vascularization) and on dynamic behavior (including fast wash-in, positive enhancement intensity, and fast wash-out) of the suspicious lesion and to allow more accurate lesion localization including mapping of hyper- and hypo-metabolic regions as well as better lesion-boundary definition. Such information might be of great value for grading the breast cancer and assessing the need for biopsy. If biopsy is needed, it could be precisely guided to the most metabolically active (*i.e.* most malignant) region.

Based on this premise, one should expect that orchestrated effort towards the development of an integrated PET and MRI breast-cancer-visualization system will result in an enhanced noninvasive diagnostic tool and will provide a useful adjunct to conventional X-ray mammography, ultrasonography, and any other clinical examination for ambiguous cases.

Multimodality coregistration and fusion of images of extracranial soft tissue is in its early stages

Address for correspondence: Andrzej Krol, Ph. D., Associate Professor of Radiology, SUNY Upstate Medical University, Department of Radiology, 750 E. Adams St., Syracuse, NY 13210, Tel.: (315) 464-7054, Fax: (315) 464-7068. E-mail: krola@upstate.edu

of development. A number of commercial devices (e.g. PET/CT, SPECT/CT) and experimental devices (e.g. PET/mammography) have become available for this purpose. They are very useful for fusing simultaneously obtained images from two modalities. However, for practical and economical reasons, MRI and PET scanners cannot be combined into one device. Therefore, the only way to obtain fused MRI/PET images is through appropriate imaging protocols and image processing.

2. MATERIALS AND METHODS

2.1. Data acquisition

Positron Emission Tomography

We have used a GE Advance BGO scanner and a GE PET-CT Discovery ST BGO scanner.

PET Methodology:

1. Fiducial markers taped to the breasts at previously-marked (before MRI scan) locations.
2. Patient positioned in prone position in the scanner with breasts dependent but constrained in a replica of MRI breast antenna made of special Styrofoam.
3. Field of view centered over breasts.
4. 10 mCi F-18 FDG injected in the medial antecubital vein (22 or 20 gauge needle) in the side that is contralateral to the breast with the suspicious lesion.
5. Transmission scan: 3 minute transmission scan with two GE-68 sources.
6. PET dynamic acquisition: 2-D with septa, 10 scans at 5 minutes each, for a total of 60 minutes.
7. Fiducial skin markers removed.
8. Reconstruction using OS-EM in 128×128 matrix, voxel size 4.25 mm, real-time random subtraction and segmented attenuation correction.

2.2. MRI Methodology

1. Philips Intera 1.5 T MRI system running 8.1.3 software with 'master gradient' hardware with Philips

clinical breast coil without quadrature detection or parallel receiver technology.

2. Locations of fiducial markers marked on the breasts.
3. Patient lies prone with both breasts suspended into a single well housing the receiver coil.
4. Intravenous line placed in antecubital vein (22 or 20 gauge needle) in the side contralateral to the breast with suspicious lesion. Gd-DTPA (Magnevist; Schering AG) is delivered (0.15 mmol/kg) at constant flow of 1.5 ml/s, followed directly by 20 ml physiologic saline solution after the Pre-Gd scan is acquired.
5. Field of view centered over breasts: 360 mm \times 360 mm, except for sagittal images that are 400 mm \times 400 mm (Table I).
6. The breast imaging sequences are listed in Table I.
7. MRI image reconstruction: Images are reconstructed by 2-D (multislice) or 3-D Fourier transforms. K-space data are 0-filled to 256 or 512 complex data points, with a small amount of apodization (ringing filter). Reconstructed image matrix sizes are either 256 \times 256 or 512 \times 512.

2.3. MRI/PET Coregistration using Deformable Model and Fiducial Skin Markers

Finite-element method (FEM) deformable tissue models have been applied to predict mechanical deformations of tissues or organs, based on biomechanical tissue properties including brain shift modeling [12], heart kinetics modeling [13], breast compression simulation, such as in X-ray mammography [14], and breast image registration [15]. However, physically-based deformable breast models are very difficult to implement, because of complex and patient-specific breast morphology and highly nonlinear (hyperplastic) and difficult-to-measure elastic properties of different types of tissues in the breast, as well as explicitly unknown boundary conditions [15].

We have developed and implemented an imaging strategy and a suitable FEM model for non-

TABLE I. Protocols used in our preliminary studies.

Technique	Resolution	tr/te/(et)	Comment
Scout in 3 planes			Locate anatomy relative to isocenter
HiRes 3-D FFE	320 \times 256 \times 120 (1.1 mm)	14/3	Isotropic 3-D for image fusion calculation
T1 AxialTSE	256 \times 256 4 mm	750/7/4	Fat suppressed, anatomy
T2 AxialTSE	256 \times 196 5 mm	5600/84/14	Accentuates fluids
Axial 3-D SPIR	320 \times 270 \times 30 (3 mm)	35/5.2	IR prep'd.; High resolution anatomy
Lt Sag 3-D SPIR	320 \times 270 \times 30 (3 mm)	35/5.2	IR prep'd.; High resolution anatomy
Rt Sag 3-D SPIR	320 \times 270 \times 30 (3mm)	35/5.2	IR prep'd.; High resolution anatomy
Dynamic GRE	320 \times 270 \times 70 (3 mm)	5.4/2.1	Pre-Gd baseline reference
Dynamic GRE	380 \times 304 \times 70	5.4/2.1	During GD-DTPA injection and 5 more measurements at 90s intervals

Philips acronyms:

FFE = Fast Field Echo (a gradient echo technique [GRE], non-steady state)

TSE = Turbo Spin Echo (a multislice spin echo technique with multiple phase encodings per TR).

SPIR = Spectral Presaturation with Inversion Recovery (fat signal suppression).

rigid coregistration of PET and MR breast images. This approach overcomes the difficulties mentioned above, because it does not require information on patient-specific breast morphology and elastic tissue properties. However, it can be applied only if the stress conditions in the imaged breast are virtually the same between PET and MRI. This is accomplished by use of identical patient support and positioning systems in both modalities. Under these conditions, the observed intermodality displacements, after rigid alignment of MRI and PET images, are predominantly due to underlying biological and physical differences in the imaging process and in the reconstruction algorithm used, including differences in the scanners' spatial distortion and resolution, and in the signal-to-noise ratio [16, 17].

Our model compensates for these dissimilarities, as well as for small discrepancies in patient positioning and for minor displacements resulting from physiological and other motion. The model can be classified as a point-based registration method, and requires a small number of non-invasive fiducial skin markers visible in PET and MRI placed on the surface of the examined breast.

The fiducial markers visible in MR are made of polyethylene tubes (2 mm I.D. and 4 mm in length), filled with diluted Magnevist and sealed. For imaging with PET, a 1 mL droplet of F-18 FDG with approximately 0.5 mCi of is deposited on a blotting paper disk, 3 mm in diameter. It is then sandwiched between two strips of medical tape, thus forming a fiducial skin marker used in PET imaging. The locations of the fiducial skin markers are permanently marked on the breast skin.

The corresponding pairs of markers are manually defined in the target (PET) and in the moving (MRI) images. The localization of markers has been performed by calculating intensity-based centroids using the method described by Wang *et alii* [18].

2. 4. FEM model construction

In the framework of 3-D FEM, the breast volume and surface are discretized (meshed) by a set of finite elements (tetrahedrons or bricks for the volume and triangles for the surface) connected through nodes located on element boundaries. First, the discrete values of multimodal displacement vectors are estimated for each pair of multimodal fiducial skin markers. A dense displacement field is then obtained using FEM, by first distributing linearly the Cartesian components of the fiducial displacement vectors over the breast surface and then doing so throughout the volume. Since the displacement interpolant can be described by the Laplace-Poisson equation

$$\nabla \cdot (\kappa \nabla u_j) = 0 \quad j = x, y, z \quad (1)$$

where κ is the pseudo conductivity with $\kappa_{\text{surface}} = 1000$ κ_{volume} , and u_x, u_y, u_z are the displacement-field com-

ponents, a unique FEM solution for displacement vectors at each node can be obtained via standard steady-state heat transfer (SSHT) FEM software [ref. ANSYS FEM package was used to perform calculations]. Displacement vectors for each location within a FEM element are interpolated using a weighted sum of the element's nodal displacements with the weights equal to the element's node shape function [19],

$$\vec{u} = \sum_{i=1}^{N_{\text{nodes}}} N_i^{el} \vec{u}_i^{el} \quad (2)$$

where N_{nodes} is the number of nodes in the element, N_i^{el} is the element's node shape function, and u_i^{el} is the nodal displacement vector. The exact FEM interpolation given by Eq. 2 is used to obtain the dense displacement field within each FEM element, which in turn was used to interpolate the image gray values via a truncated sinc interpolation kernel. We call this process warping of the floating (moving) image to the fixed (target) image.

The patient-specific geometry of the breast was obtained from MRI. After breast surface segmentation, meshing was performed using the ANSYS FEM software package. The following elements were chosen from the ANSYS library: SOLID70 (Tetrahedral Thermal Solid) for the bulk of the breast volume, and SHELL57 (2-D Thermal Shell) for the breast surface.

3. RESULTS

3. 1. Phantom results

To estimate the performance of our method, first we imaged a custom-manufactured deformable breast phantom (CIRS Inc., Norfolk, VA; www.cirsinc.com), filled with medium-stiffness gel (vinyl-based hydrophobic polymer with low concentration of nickel chloride) and surrounded by a skin made of thin urethane foil. Breast 'lesions' visible in MRI were emulated by injection of oil. F-18-FDG diluted in water-soluble gelatin with organic dyes was injected as close as possible to the 'lesions' that emulated lesions visible in PET. Six internal 'lesions' could be uniquely identified in both PET and MRI. The fiducial skin markers were used as described above. The phantom was imaged using PET and MRI techniques described above. The SSHT FEM model was implemented and nonrigid deformation of the MRI phantom image to PET image was performed. The Target Registration Error (TRE) for different lesions was estimated and the results are collected in Table II. We observe that the TRE is comparable with the PET voxel size (4.25 mm).

3. 2. Patient results

We have acquired PET and MRI data with fiducial skin markers on a few patients, using the protocols and the processing methodology described above.

TABLE II. Target registration errors (TRE in mm) calculated using all markers.

Lesion	x_{obs}	x_{est}	y_{obs}	y_{est}	z_{obs}	z_{est}	TRE
1	1.05	1.19	0.51	-0.91	-9.40	-4.69	4.92
2	1.99	0.29	2.15	-0.92	-6.49	-3.53	4.58
3	-1.92	0.34	-1.99	-0.11	1.35	-0.69	3.57
4	0.63	0.21	2.89	0.13	2.22	-1.37	4.55
5	-0.41	-0.67	-0.93	-0.86	-4.79	-4.57	0.34
6	-1.99	-0.19	-2.15	-0.41	1.06	0.65	2.54

We have applied our SSHT FEM coregistration technique to perform the multimodal PET/MRI. The high-resolution MRI scan, currently obtained for anatomical purposes, also works very well for defining the surface of the breast. This 3-D T1 weighted sequence has been obtained without fat saturation, so that the skin surface is easily visualized. It permits automated computer segmentation via simple thresholding with good definition of the breast surface. Similarly, in images obtained in the dynamic GRE MRI acquisition series, breast skin is well defined and can be easily segmented out via thresholding. The segmented breast surface was used to create the FEM mesh with the ANSYS package. The geometric centroids of fiducial markers visible in PET and MRI were estimated using the iterative method described above, and the discrete displacement field was obtained. These data allowed our FEM model to obtain a dense displacement field (*i.e.*

a displacement vector for each mesh node), which in turn was used to warp in 3-D the moving MRI image to the target PET image. Coregistered images were fused using the Analyze package. In addition, we estimated various similarity measures for coregistered images before and after registration (Table III).

Examples of the patient mesh, displacement field distribution, and coregistered and fused PET/MRI images are shown in Figures 1-3. We coregistered and fused prone high-resolution (HiRes) 3-D Fast Field Echo (FFE) MRI with F-18-FDG prone PET. Our method (Figure 3a) yielded improved coregistration of the enhanced metabolic activity region revealed by PET with the well-defined lesion demonstrated by HiRes MRI (Figure 3c), as compared to pure rigid registration (Figure 3b). It is possible now to determine which part of the lesion is metabolically hyperactive.

4. CONCLUSIONS

The SSHT deformable FEM breast model performs well for PET/MRI breast image registration if the stress conditions in PET and MRI are similar. The registration procedure requires a) fiducial skin markers surrounding the suspicious lesion, b) that a replica of MRI breast antenna be used during the PET scan, and c) very careful patient positioning to prevent variation in the internal stress condition between PET and MRI.

TABLE III. Calculated image similarity measures.

Patient # FEM node/element number	Best case is 2.0 for NMI, and 1.0 for NCC.			
	NMI before	NMI after	NCC before	NCC after
#1 26,569/17,247	1.0687	1.3312	0.2894	0.3557
#2 25,832/19,646	1.0943	1.1346	0.2056	0.2675
#3 22,805/14,652	1.0594	1.2527	0.4289	0.4311

NMI denotes normalized mutual information.
NCC denotes normalized correlation coefficient.

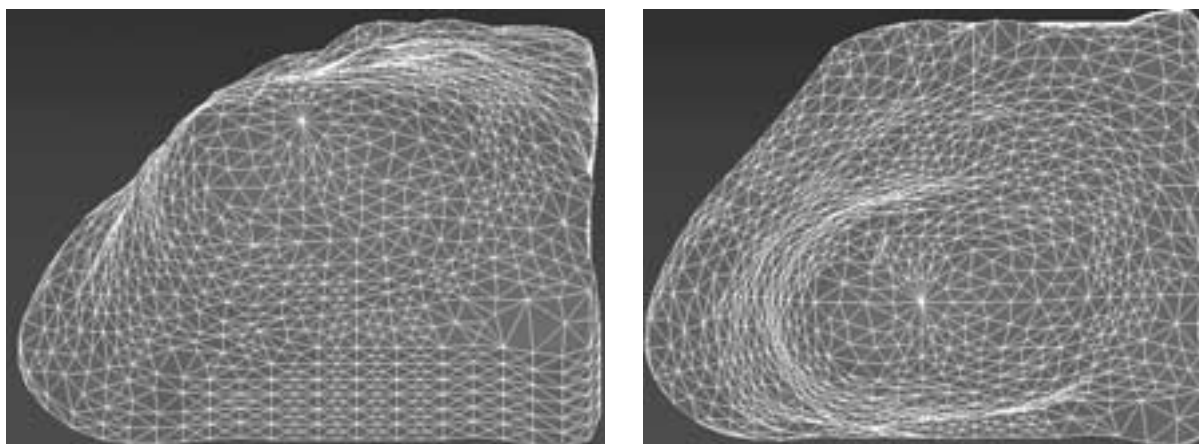


FIG. 1. Mesh generated for patient #1: a. 60° view; b. top view.

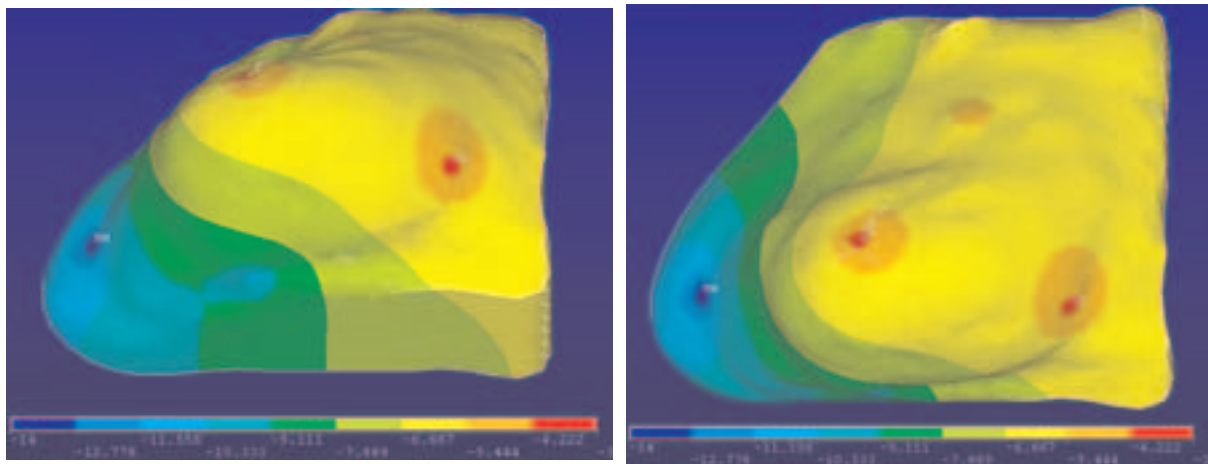


Fig. 2. Displacement field component calculated by our SSHT FEM model for patient #1: a. 60° view; b. top view.

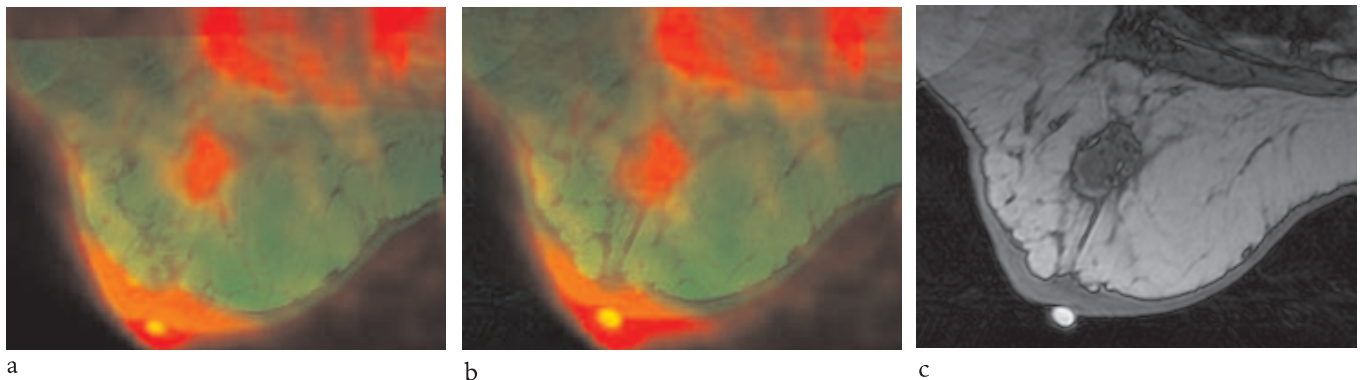


Fig. 3. Coregistered and fused images of patient #1 (transaxial slice 120; red channel = PET; green channel = high-resolution 3-D FFE MRI with pixel size 0.7 mm). a. after SSHT FEM registration. b. after rigid registration. c. MRI only.

REFERENCES

[1] American Cancer Society 2002. Cancer Facts and Figures <http://www.cancer.org>

[2] Bloomstone M, D'Angelo P, Galliano D *et alii*. One Hundred Consecutive Advanced Breast Biopsy. *Annals Sur Onc* 1999; 6; 195-199.

[3] Burkhardt J H, Sunshine J H. Core-Needle and Surgical Breast Biopsy: Comparison of Three Methods of Assessing Cost. *Radiology* 1999; 212; 181-188.

[4] Philpotes L E, Hooley R J, Lee C H. Comparison of Automated Versus Vacuum-Assisted Biopsy Methods for Sonographically Guided Core Biopsy of the Breast. *AJR* 2002; 180; 347-351.

[5] Baines C J. Menstrual Cycle Variation in Mammographic Breast Density. *J Natl Cancer Inst* 1998; 90; 875.

[6] Bombardieri E, Crippa F. PET imaging in breast cancer. *Quat J Nuc Med* 2001; 45; 245-256.

[7] Wahl W R. Current Status of PET in Breast Cancer Imaging, Staging, and Therapy. *Seminars in Roentgenology* 2001; 36; 250-259.

[8] Palmedo H, Hensel J, Reinhardt M, Von Mallek D, Matthies A, Biersack H J. Breast cancer imaging with PET and SPECT agents: an in vivo comparison. *Nucl Med and Biol* 2002; 29; 809-815.

[9] Scheidhauer K, Walter C, Seemann M D. FDG PET and other imaging modalities in the primary diagnosis of suspicious breast lesions. *Eur J Nucl Med Mol Imaging* 2004; 31 (Suppl 1); S70-S79.

[10] Eliat P A, Dedieu V *et alii*. Magnetic resonance imaging contrast-enhanced relaxometry of breast tumors: an MRI multicenter investigation concerning 100 patients. *Mag Res Imaging* 2004; 22, 475-481.

[11] Gibbs P, Liney G P *et alii*. Differentiation of benign and malignant sub-1 cm breast lesions using dynamic contrast enhanced MRI. *Breast* 2004; 13; 115-121.

[12] Castellan-Smith A, Hartkens T, Schnabel J *et alii*. Lecture Notes in Computer Science. *Proc Med Img Comp Comp Ass Inter* 2001; 2208; 1091-1098.

[13] Sitek A, Klein G J, Gullberg G T *et alii*. Deformable Model of the heart with Fiber Structure. *IEEE TNS* 2002; 49; 789-793.

[14] Azar F S, Metaxas D N, Schnall M D. A Deformable Finite Element Model of the Breast for Predicting Mechanical Deformations under External Perturbations. *Acad Radiol* 2001; 8; 965-975.

[15] Samani A, Bishop J, Plewes D B. A Constrained Modulus Reconstruction Technique for Breast Cancer Assessment. *IEEE Trans Med Imaging* 2001; 20 (9); 877-885.

[16] Jazzard P. Physical Basis of Spatial Distortion in MRI. In: *Handbook of Medical Imaging*. I N Bankman Ed. Academic Press 2000.

[17] Dahlbom M, Huang C. Physical and Biological Bases of Spatial Distortion In PET Images. In: *Handbook of Medical Imaging*. I N Bankman Ed. Academic Press 2000.

[18] Wang M Y, Maurer C R, Fitzpatrick J M *et alii*. An Automatic Technique for Finding externally Attached markers in CT and MRI volume images of the head. *IEEE Trans Biomed Eng* 1996; 43; 627-637.

[19] Zienkiewicz O C, Taylor R L. *The Finite Element Method*. New York. McGraw Hill Book Co 1987.